

“Fabrication and Characterization of Silicon Nanowires”

By

Rupnayan Borah



**DISCIPLINE OF PHYSICS
INDIAN INSTITUTE OF TECHNOLOGY INDORE**

June 2015

“Fabrication and Characterization of Silicon Nanowires”

A THESIS

*Submitted in partial fulfillment of the
requirements for the award of the degree
of*
Master of Science

by
Rupnayan Borah



DISCIPLINE OF PHYSICS
INDIAN INSTITUTE OF TECHNOLOGY INDORE
JUNE 2015



INDIAN INSTITUTE OF TECHNOLOGY INDORE

CANDIDATE'S DECLARATION

I hereby certify that the work which is being presented in the thesis entitled “**Fabrication and Characterization of Silicon Nanowire**” in the partial fulfillment of the requirements for the award of the degree of **MASTER OF SCIENCE** and submitted in the **DISCIPLINE OF PHYSICS, Indian Institute of Technology Indore**, is an authentic record of my own work carried out during the time period from August, 2014 to June, 2015 under the supervision of **Dr. Rajesh Kumar and Dr. P.R. Sagdeo, Assistant Professor**.

The matter presented in this thesis has not been submitted by me for the award of any other degree of this or any other institute.

Signature of the student with date
(Rupnayan Borah)

This is to certify that the above statement made by the candidate is correct to the best of my/our knowledge.

Signature of the Supervisor of
M.Sc. thesis #1 (with date)
(Dr. Rajesh Kumar)

Signature of the Supervisor of
M.Sc. thesis #2 (with date)
(Dr. Pankaj R. Sagdeo)

Rupnayan Borah has successfully given his/her M.Sc. Oral Examination held on <**Date of M.Sc. Oral Examination**>.

Signature(s) of Supervisor(s) of MSc thesis
Date:

Convener, DPGC
Date:

Signature of PSPC Member #1
Date:

Signature of PSPC Member #1
Date:

ACKNOWLEDGEMENTS

I wish to thank my supervisors Dr. Rajesh Kumar and Dr. P.R. Sagdeo for their valuable guidance, useful comments and remarks. I am also grateful to Dr. Gayatri sahu for her support.

I would also like to thank Mr. Shailendra Saxena for his kind support.

I would also like to thank the PSPC members Dr. Preeti Bhobe and Dr Sanjay Singh.

I want to acknowledge Ms. Priyanka Yogi, Mr Ashish Kumar and Mr. Tejendra Kumar for helping me in conducting my experiments smoothly.

I thank my seniors and colleagues Mr. Hari Mohan Rai, Mr. Ravikiran Late and Mr. Suryakant Mishra, Mr. Vikash Mishra, Mr. Md Balal and Mr. Kamal Warshi for beautiful moments that kept our laboratory a beautiful place to work. With their presence, research work was more than enjoyable.

Words are inadequate to express my emotional gratitude towards my friends Ms. Anupriya, Mr. Ashish, Mr. Rohit, Mr. Uttiya, Mr. Ravi Kumar, Mr. Sahidul Mondal, Mr. Sourabh Solanki and Mr. Jigar Chaudhary for encouraging me to do my research.

I am also thankful to Sophisticated Instrumentation Centre (SIC) at IIT Indore for Photoluminescence and SEM measurements. I never felt any difficulties to carry out this experiment.

It is their help and support, due to which I became able to complete this technical report. Without their support this report would not have been possible.

Rupnayan Borah

M.Sc. II Year

Discipline of Physics

IIT Indore

Dedicated to
My family and teachers

Abstract

Well aligned Silicon (Si) nanowires (NWs) are successfully fabricated by metal induced etching (MIE) technique. Effect of etching time on the porosification of Si has been studied. The effect of Silver nanoparticles (AgNPs) deposition time on the the porosification of Si has also been studied. Image J software is used to estimate the porosity of different samples. It is observed that porosity of samples (containing SiNWs) increases as AgNPs deposition time (prior to porosification) increases. The optimized parameter for the fabrication of SiNWs has been discussed. Photoluminescence (PL) has been carried out to see quantum confinement effect in SiNWs samples. Raman spectroscopy has been utilized to confirm the presence of nanostructures in the samples. Asymmetrically broadened Raman spectra are observed from SiNWs samples. Bond polarizability model (BPM) is used to estimate the SiNWs size present in the samples from Raman scattering data. This study is important to understand the mechanism of fabrication of SiNWs and their properties.

TABLE OF CONTENTS

LIST OF FIGURES

LIST OF TABLES

ACRONYMS

Chapter 1: Introduction	1
Chapter 2: Theoretical Background	
2.1 Overview of Silicon	3
2.2 Quantum confinement effect	5
2.3 Synthesis of SiNWs	
2.3.1 Chemical vapour depositon	6
2.3.2 Molecular beam Epitaxy	6
2.3.3 Laser Ablation Method	7
2.3.4 Metal Induced Etching	7
2.4 Characterizing techniques	
2.4.1 Scanning Electron Microscopy	7
2.4.2 Photoluminiscence	10
2.4.3 Raman Spectroscopy	12

Chapter 3: Experimental Details	
3.1 Sample preparation	15
3.2 Mechanism for formation of SiNWs	16
3.3 Raman and PL Spectroscopies	18
Chapter 4: Results and Discussions	
4.1 SEM Image analysis	19
4.2 Effect of etching time on porosification of Si	22
4.3 Spectroscopic Investigation of SiNW samples	
4.3.1 Photoluminiscence study of the samples	27
4.3.2 Raman Study of the samples	29
4.4 Effect of AgNPs deposition time on porosificataion of Si wafer	31
Chapter 5: Conclusions	37
APPENDIX-A	38
APPENDIX-B	43
REFERENCES	44

LIST OF FIGURES

- Fig. 2.1** Silicon crystal structure
- Fig. 2.2** E-**k** diagram showing direct band gap
- Fig. 2.3** E-**k** diagram showing indirect band gap
- Fig. 2.4** A schematic diagram for SEM
- Fig. 2.5** A schematic diagram for components coming out of a sample in SEM
- Fig. 2.6** Experimental set up for PL measurements
- Fig. 3.1** Schematic diagram for the formation of SiNWs
- Fig. 4.1** SEM image of bare n type Silicon substrate
- Fig. 4.2** Ag deposited on n-type Si substrate
- Fig. 4.3** SEM image of porosified Ag deposited Si wafer
- Fig. 4.4** Cross-sectional view of SiNWs prepared from n-type Si wafer
- Fig. 4.5** Top view of etched p-type Si wafer for 60 min
- Fig. 4.6** Cross-sectional SEM image of SiNWS formed on p - type Si substrate
- Fig. 4.7** Top view SEM image of sample (a) E1, (b) E2 and (c) E3
- Fig. 4.8** Cross-sectional view of sample (a) E1 (b) E2 and (c) E3
- Fig. 4.9** PL spectra for sample (a) E1 (b) E2 and (c) E3
- Fig. 4.10** Raman spectra for sample (a) E1 (b) E2 and (c) E3

Fig. 4.11 SEM images of n ($0.01\Omega\text{cm}$) type Si substrate. Sample A to D showing variation in AgNPs.

Fig. 4.12 SEM image of sample (a) A60, (b) B60 (c) C60 and (d) D60

Fig. 4.13 Variation of covered area with Ag NPs deposition time.

Fig. 4.14 Variation of porosity with Ag NPs deposition time

LIST OF TABLES

- Table I : Specification of samples for studying effect of etching on porosification of Si
- Table II : Specification of the porous silicon samples prepared with n type (0.01 Ω cm) Si substrate
- Table III: Specification of the porous silicon samples prepared with n type (0.01 Ω cm) Si substrate with only AgNPs deposition
- Table IV: Specification of the porous silicon samples prepared n type (0.01 Ω cm) substrate after etching

ACRONYMS

Acronym	Meaning
SiNW	Silicon Nanowire
PL	Photoluminescence
SiNs	Silicon Nanostructures
TNT	Trinitrotoluene
RDX	Research Department Explosives
CVD	Chemical Vapour Deposition
MBE	Molecular Beam epitaxy
MIE	Metal Induced Etching
SEM	Scanning Electron Microscope
IPA	IsoPropyl Alcohol
PS	Porous Silicon
CIF	Centre for Instrumentation Facility
SIC	Sophisticated Instrument Centre

Chapter 1

Introduction

Silicon nanostructures (SiNs) are very important mostly due to its light emission properties [1, 2]. SiNs are still of research interest due to its unique properties and applications [1–7]. Literatures reports applications of SiNs in advanced sensing [8–11], in making electrodes for batteries [12,13], in carrying out mass spectroscopy[14] and in field effect transistors [15,16]. SiNWs configured as field effect transistors have been demonstrated to detect explosives including TNT and RDX [17]. Based on confinement, SiNs are of mainly three type which includes Si nano sheet (one dimensional confined), nanowires (two dimensional confined) and nanodots (three dimensional confined).

Si nanowires (NWs) are one of the most attractive nanostructure which is drawing more attention of researchers looking for application in nanotechnology [15,18]. SiNWs are 1D nanostructures i.e. it is two dimensionally quantum confined which leaves one unconfined direction for electrical conduction which makes it a possible candidate to be used in applications where electrical conduction is required. Their unique optical, electrical, thermal and magnetic properties make them quite significantly different from their 3D bulk counterpart [19]. In comparison with bulk Si, SiNWs have greater surface to volume ratio. As a result on reducing the size, the number of surface atom increases. Optical absorbance depends on surface atoms and so increment in number of surface atoms increases its optical absorbance which implies that SiNWs have more optical absorbance than bulk Si. The optical absorbance of SiNWs is highest in larger wavelengths [20]. Band gap increases with the decrease in the size of SiNs as it depends on the diameter of the nanowire. When there is less neighboring atoms, there will be less cohesive energy between them so cohesive energy of the SiNWs is less than its bulk counterpart because as a result of reduction of size, number of surface atoms decreased. These various aspects of physical, chemical

and mechanical properties of SiNWs make them a promising candidate for optoelectronics. Si optoelectronics devices can be made due to strong photoluminescence (PL) in optical region is observed at room temperature from nanowires.

It is known that when the diameter of a semiconductor is reduced to the same order as the Bohr's exciton radius, quantum confinement effect occurs and the exciton properties get modified. In a quantum wire or nano-wire, excitons are confined in two dimensions and are free in only one dimension. In case of Quantum well the excitons are confined in only one directions and so free to move in any two directions. Basically, the bandgap increases in all cases because the allowed energies are pushed up by quantum confinement effectively. As the nanoparticle size becomes smaller the up-shift of the quantum confined bandgap also increases. Having such tremendous promise it is important to understand the formation of SiNWs, investigate its different optical and electronic properties, so with the help of this information its potential for industrial applications could be exploited

Fabrication of SiNWs to a dimension where quantum confinement effect occurs is very important in order to explore its properties and morphology. Various methods are available by which we can fabricate SiNs/SiNWs. Various fabrication techniques to fabricate SiNWs and the properties of fabricated NWs have been discussed in following chapters.

CHAPTER 2

Theoretical background

2.1 Overview of Silicon

This era may be called as the “Nano age” because of the numerous amount of research going on in nanotechnology. SiNWs are the part of this age whose promises are profound. The impact of SiNWs on different fields may improve the society and our future for good. As discussed earlier, the properties of SiNWs are very much different from their bulk counterpart. In this section we will broadly discuss about the properties of Si and different synthesis method of SiNWs.

Being the second most abundant element on earth, Si is most used material in electronic devices. It occurs naturally as oxides and silicates. Silicon crystallizes in the same pattern as diamond, in a structure known as "two interpenetrating face-centered cubic" primitive lattices as shown in Fig. 2.1. The lines between silicon atoms in the Fig 2.1 indicate nearest neighbor bonds. Different properties of Si are listed in the Appendix-I.

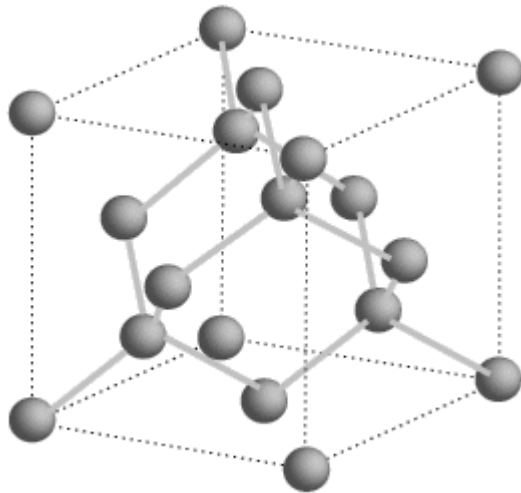


Fig.2.1 Silicon Crystal structure

As discussed above, the electronics' market is ruled by Si and the whole microelectronics industry is dominated by Si. It has a band gap of 1.1 eV and the essential and best dielectric required for device formation is possessed by Si. Moreover, Si is non-toxic, relatively inexpensive, easy to process, and has good mechanical properties. Because of all these reasons, it is considered the best material in electronic systems. But due to its inefficiency in emitting light, bulk Si is not ideal for use in optoelectronic applications. The reason behind its inability to use for optoelectronic applications is its indirect energy band gap. Indirect energy bandgap in a semiconductor means, the maximum of the valence band and the minimum of the conduction band do not occur in the same value of \mathbf{k} in the \mathbf{k} -space. Fig. 2.2 and Fig. 2.3 shows the indirect band gap and the direct band gap transitions respectively in semiconductors. In an indirect semiconductor momentum conservation does not allow the recombination by a single photon which possesses negligible momentum. Therefore, momentum conservation takes place via phonon. Light emission efficiency is very less in bulk because non radiative process dominates over the phonon assisted optical transition. Bulk silicon is therefore not suitable for the fabrication of optoelectronic devices.

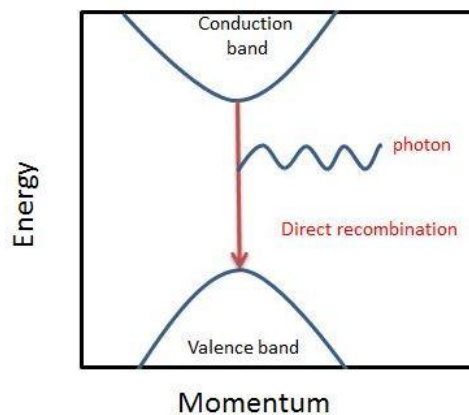


Fig 2.2 E- \mathbf{k} diagram showing direct band gap

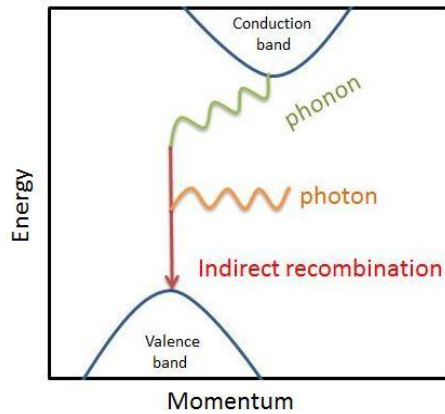


Fig 2.3 E-**k** diagram showing indirect band gap

2.2 Quantum Confinement Effect

Quantum confinement effect occurs when size of crystal becomes less than the corresponding Bohr exciton radius as already discussed in chapter 1. NSs properties change with the change in degree and dimensionality of confinement. Three types of confined structures have been defined based upon the dimensions which are Quantum well, Quantum wire and Quantum dot. Quantum well, Quantum wire and Quantum dot shows confinement in two, one and zero dimensions respectively.

Indirect band gap can be changed into direct band gap with the help of quantum confinement. Si have indirect band gap and hence does not give any luminescence at room temperature. But nanostructures of Si due to quantum confinement gives PL at room temperature. With the help of uncertainty principle the conversion of indirect band gap to direct band gap can be understood. Let the uncertainties in the position and wave vector be Δx and Δk respectively. According to uncertainty principle, $\Delta k \cdot \Delta x \sim 1$. Δx is infinity in bulk materials because of its crystalline nature. Hence, by uncertainty principle only possible transitions is $\Delta k = 0$. Suppose the size of a NS is L then there will be an uncertainty of $1/L$ in the

momentum due to uncertainty in position being 'L'. When Δk lies in the range of $1/L$ all the transitions are possible. Thus, optical recombination occurs in suitable low dimensional materials. Consequently, for optical transitions to take place, band gap can be said to be effectively a direct type in nature.

2.3 Synthesis of SiNWs

SiNWs was first synthesized successfully in 1950's [21] by Treuting et al. of unknown diameter. Different approaches have been tried since then. Numerous ways have been developed to synthesize SiNWs, including both the bottom-up and the top-down approaches.

Most commonly used methods are described below:

2.3.1 Chemical Vapor Deposition

Chemical Vapor Deposition (CVD) is a cost effective method [22] in which the source material used to grow SiNWs is SiO. SiO granules are taken in crucible of a tube furnace and inert gas supply is given to the tube furnace. The furnace is maintained at 1350°C . Si gets evaporated at this temperature in the furnace and flows from hotter end to the cooler part which leads to the formation of SiNWs. The disadvantage of this technique is the byproduct of CVD reactions which can be hazardous and the requirement of high temperature.

2.3.2 Molecular Beam Epitaxy

Molecular Beam Epitaxy uses highly pure Si source and is heated till Si evaporates [22]. Ultrahigh Vacuum is required to reduce the contamination and easy evaporation. After heating a gaseous beam of Si atoms is obtained which is directed towards the substrate and SiNWs are fabricated. The main disadvantage of this method is that it requires expensive experimental setup.

2.3.3 Laser Ablation Method

In laser ablation method a pulsed laser is used. By this process ultra-thin SiNWs is obtained [22]. Heat is applied to the target material placed in a tube furnace. Now the pulsed laser source is used to ablate the target material. After that cooling down of the ablated Si material occurs when it collides with the inert gas molecule. Si nano droplets are formed when Si vapor condenses. Consequently, Si nanowires are formed when these Si nano droplets falls on the substrate.

2.3.4 Metal Induced Etching

Metal Induced Chemical Etching [23] is a simple and low-cost method for the fabrication of various Si nanostructures with the ability to control various parameters. It is a novel wet-etching technique. The elements commonly used in this etching method for deposition in Si substrate are Ag, Au, Pt etc. SiNWs are prepared by this method by dipping Si wafer in AgNO_3 and HF solution for the deposition. Si gets oxidized by the Ag^+ ion present in the solution by taking electron and produces SiO_2 . Due to HF the SiO_2 is etched away and the Si under Ag particles are etched away faster. Ag particles are then removed from the substrate using HNO_3 leaving SiNWs. This technique can be used to fabricate SiNWs in both n and p type Si substrate.

2.4 Characterizing Techniques

2.4.1 Scanning Electron Microscope (SEM)

The scanning electron microscope (SEM) is an instrument that produces a largely magnified image by using electrons instead of light to form an image. It can magnify objects upto 300,000 times the size of the object studied.

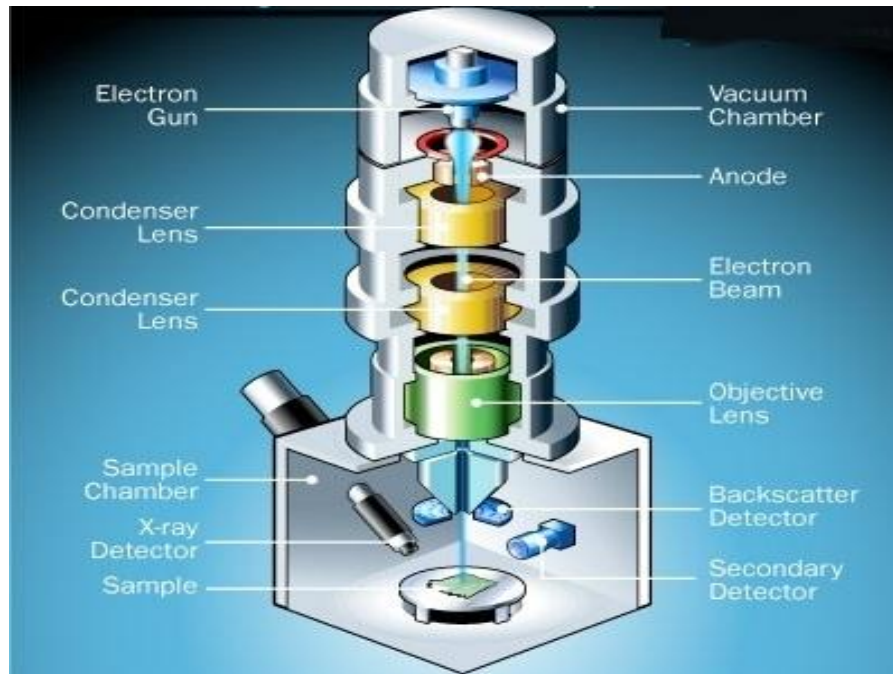


Fig. 2.4 A schematic diagram of an SEM [24]

An SEM consists of electron gun, vacuum chamber, lenses, detectors and sample chamber as shown in Fig . The electron gun is the filament which is the source of the beam of the electrons. The filament is made of tungsten and is heated to generate a high beam of electrons. Generally, it is of V-shaped. High electric field at the very sharp tip causes electrons to tunnel through the barrier. If the filament is overheated or too old, it will break.

The lenses used in SEM are not made of glasses instead they are actually made of magnets. These magnets have the capability to bend the path of electrons and control the flow of electrons and makes sure that the electron beam falls on the right area where it is needed. It actually works like the focusing lenses of an optical microscope. Then comes the sample chamber which is kept still. SEM

images can get deteriorate if sample chamber is not steady since SEM's are sensitive to vibrations. So to get clear images they are insulated from vibrations.

The vacuum chamber is an utmost necessary for an SEM. Without vacuum there will be air particles inside the chamber. When the electron beam is fired by the electron gun , the air particles will come in their way and block their path due to which electron beam will get scattered before reaching the sample. The surface of the sample may also get distorted due to knocking down of the air particles from the air and onto the sample.

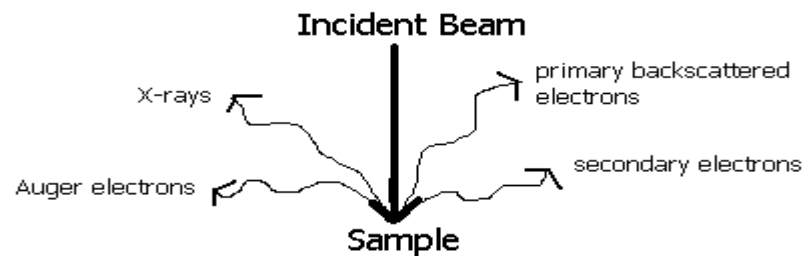


Fig. 2.5 Schematic of the components coming out of sample.

The electron beam produced by the electron gun at the top of the microscope is made to travel through the vacuum focused by the electromagnetic lenses and allowed to fall on the sample. When the beam strikes the sample, electrons and X-rays are scattered as shown in Fig 3. These X-rays, primary backscattered and secondary electrons are collected by the detectors attached to the SEM. The detectors convert this analog signal into digital through an analog to digital convertor and send to the computer. The computer then converts this digital signal into grayscale pixels which produces the final image. It is called scanning electron microscope because dot by dot, row by row, an image of the original object is scanned onto a monitor for viewing. To magnify an image only a small portion of the image is to be scanned.

2.4.2 Photoluminescence

Luminescence is the radiative emission process from a solid. Photoluminescence (PL) is a process of emission of light from a material when it is subjected to UV light. The process involves excitation of photon and hence known as photoluminescence. In general, the PL involves excitation and relaxation processes during the absorption and emission of photons.

The excitation energy and intensity are chosen to probe different regions and excitation concentrations in the sample. PL investigations can be used to characterize a variety of material parameters. PL spectroscopy provides an extremely sensitive probe of discrete electronic states. Features of the emission spectrum can be used to identify surface, interface, impurity levels and interface roughness. The intensity of the PL signal provides information on the quality of surfaces and interfaces.

When light of sufficient energy is incident on a material, photons are absorbed and electronic excitations are created. Eventually, these excitations relax and the electrons return to the ground state. If radiative relaxation occurs, the emitted light is called PL. This light can be collected and analyzed to yield a wealth of information about the photoexcited material. The PL spectrum provides the transition energies, which can be used to determine electronic energy levels. The PL Intensity gives a measure of the relative rates of radiative and nonradiative recombination. Variation of the PL intensity with external parameters like temperature and applied voltage can be used to characterize further the underlying electronic states and bands [25].

PL depends on the nature of the optical excitation. The excitation energy selects the initial photoexcited state and governs the penetration depth of the incident light. The PL signal often depends on the density of photoexcited electrons, and

the intensity of the incident beam can be adjusted to control this parameter. When the type or quality of material under investigation varies spatially, the PL signal will change with excitation position. In addition, pulsed optical excitation provides a powerful means for studying transient phenomena. Short laser pulses produce virtually instantaneous excited populations, after which the PL signal can be monitored to determine recombination rates. PL analysis is an important tool for the characterization of surfaces, because the PL signal is often originated near the surface of a material. The presence of surface adsorbates alters the intensity of the PL signal. When the states serves long-lived traps, then the depth of the trap can be determine by the temperature dependent PL. If interface states are nonradiative, which is usually the case, the states alter the time-resolved PL of radiative transitions in the material. Nonradiative traps dominate the transient PL signal at low carrier density.

The schematic of the set up for photoluminescence detection is shown in fig4. The carriers are excited in the sample using suitable laser beam. The photoluminescence coming out from the sample is detected as shown in Fig. 3.4.

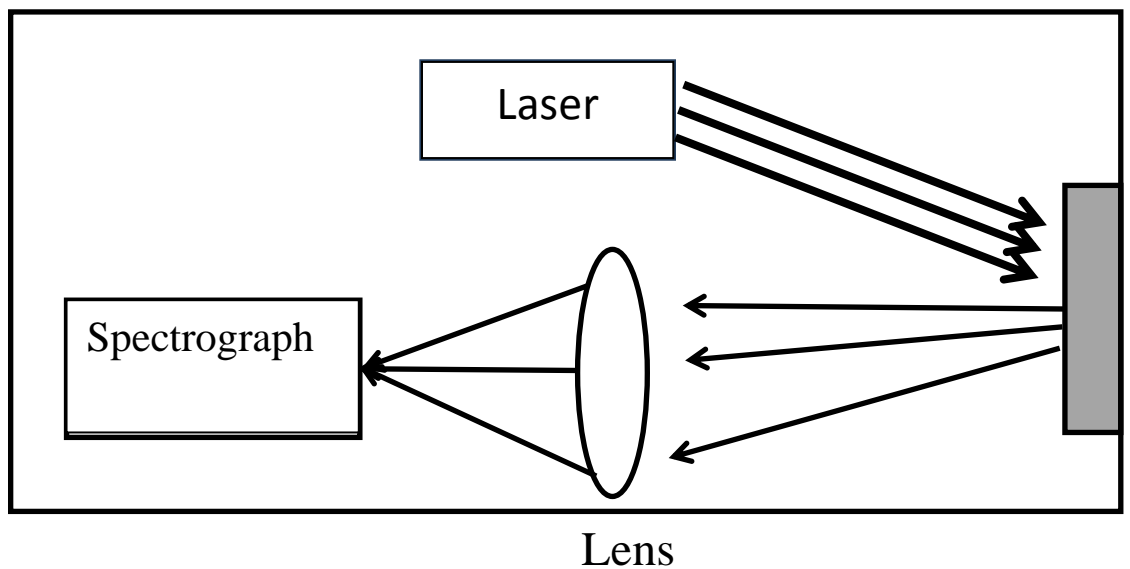


Fig. 2.6 Experimental set-up for PL measurements.

2.4.3 Raman Spectroscopy

Raman spectroscopy is a spectroscopic technique based on inelastic scattering of monochromatic light, usually from a laser source. It can be used to study solid, liquid and gaseous samples. It is named after the nobel laureate Sir Chandrasekhar Venkata Raman who discovered Raman effect in 1928. This discovery was quite remarkable because he detected this feeble phenomenon with sunlight as source, telescope as collector and his own eyes as detector.

When a monochromatic light beam is deflected by molecules or crystal lattices intense spectral line occurs corresponding to the wavelength of incident light. However, besides these lines, additional lines occurs through spectral analysis which are weaker but corresponding to wavelengths different from the incident light. These lines are known as Raman lines and the phenomenon due to which these weaker lines are observed is called Raman effect. The lines corresponding to the wavelength of incident light are known as Rayleigh lines.

A classical explanation of Raman effect can be given based on molecular deformations in electric field E due to the molecular polarizability α . The light source which is generally a laser beam can be considered as an oscillating electromagnetic wave with electrical vector E . When the light is made to fall upon the sample an electric dipole moment is induced due to the interaction which deforms molecules. Let the dipole moment be $P = \alpha E$. Now due to this deformation, vibration of molecules results with a particular frequency, say ν_m .

Molecules of the samples illuminated by light source gets excited with a frequency ν_0 and is transformed into oscillating dipoles. Three different frequencies of light can be emitted by such oscillating dipoles which are mentioned below:

1. Emmision of light can happen when a photon with the frequency ν_0 is absorbed by a molecule with no Raman-active modes. This molecule after getting excited comes back to the same basic vibrational state. Thus, light with the same

frequency ν_0 is emitted as an excitation source. This type of scattering is called an elastic Rayleigh scattering.

2. A Raman-active molecule absorbs a photon with frequency ν_0 which was in the basic vibrational state while interacting. Part of the photon's energy is transferred to the Raman-active mode with frequency ν_m and the resulting frequency of scattered light is reduced to $\nu_0 - \nu_m$. This Raman frequency is called Stokes frequency, or just "Stokes".

3. A Raman-active molecule absorbs a photon with frequency ν_0 , but it was already in the excited vibrational state while interacting with the sample. Molecules while returning to the basic vibrational state releases excessive energy, and scattered light gives a frequency of $\nu_0 + \nu_m$. This type of Raman frequency are called Anti-Stokes.

Two discrepancies has been seen in the classical explanation of Raman effect:

(1) According to the this theory, the Raman frequencies above and below the Rayleigh line must be of the same intensity, but this is not consistent with the experimental observation.

(2) It cannot explain the independence of Raman shift from incident laser wavelength

The major components that make up the Raman spectrometer are the following [14]:

- (1) Excitation Source
- (2) Sample illumination and collection system
- (3) Wavelength selector
- (4) Detector and computer control system

Excitation sources: Ideal excitation source for Raman Spectroscopy are lasers because it can produce laser beams in wide wavelength and also provide power upto 1-2W. Moreover, laser beams being completely linearly polarized add to its advantage. Earlier in 1960s mercury lamp was used as an excitation source. The main lasers that are used in raman spectrometer are Continuous wave gas lasers, Neodymium-YAG lasers, Diode lasers and Tunable lasers.

Wavelength selector: In order to obtain a certain wavelength or a narrow band of wavelengths, wavelength selectors are used. For this reason this instrumental component is very important. It can be classified into several categories eg. filters, prisms etc. Raman Spectra is measured extensively using both prism and grating monochromators and spectrographs. However, acoustic and liquid-crystal tunable filters have also been used recently with success.

Detection: The most used detector in Raman spectroscopy is charge-coupled devices (CCDs). A CCD is a silicon based multichannel array of photosensitive elements, each one of which generates photoelectrons and store them as a small charge. It is mainly used because of its sensitivity to light which makes it suitable for inherently weak Raman signal analysis.

CHAPTER 3

Experimental Details

3.1 Sample Preparation

The method adopted for fabricating SiNWs for the project work is metal induced chemical etching. It is one of the simple and low cost methods for this purpose. In this method, the materials and chemicals used are Si wafer, HF, AgNO₃, H₂O₂ and HNO₃ [23,26]. The steps involved in sample preparation are discussed below.

Step 1: The silicon wafer is cut into pieces with a diamond cutter and then these silicon wafers are ultrasonicated in IPA for 10 minutes and then again for another 10 minutes in acetone to remove the organic contaminants on the surface.

Step 2: The cleansed Si wafer are dissolved in a 5% HF solution. This process is done to remove the thin oxide layer that is formed on the surface of the silicon wafer due to exposure with air.

Step 3: After removing the oxide layer it is dipped into the solution containing 4.8M HF and 0.005M AgNO₃ for 1 minute at room temperature for the deposition of Ag nanoparticles and then it is rinsed with deionized water to remove the extra silver ions.

Step 4: The AgNPs deposited samples were then kept for etching in an etching solution containing 4.6 M HF & 0.5 M H₂O₂. The samples were kept for different times.

Step 5: The Ag metal was dissolved with nitric acid which was immersed into 5% HF solution to remove the oxide layer induced by the nitric acid. Finally, the wafers were cleaned with water.

Detailed mechanism and reactions resulting in SiNWs are discussed in the next section.

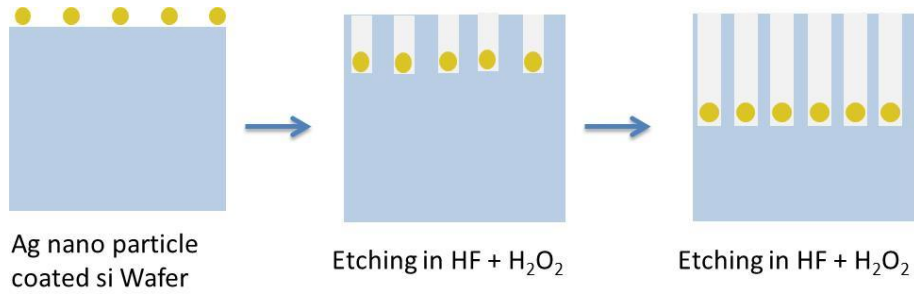
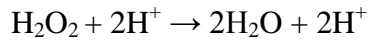


Fig. 3.1 Schematic diagram of the formation of SiNWs

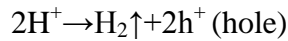
3.2 Mechanism for the formation of SiNWs

Mechanism for the formation of SiNWs are discussed below:

A) The etching of Si wafer in a solution containing HF and H_2O_2 is a redox reaction. The cathode reaction is given by:

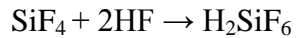


B) Another cathode reaction happens simultaneously which is reduction of protons into hydrogen. It was proposed by Li and Bohn and Harade et.al [27].

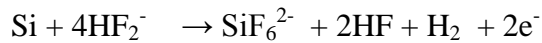


C) The anode reaction proposed in this method can be divided into three groups:

1) Direct dissolution of Si in tetravalent state

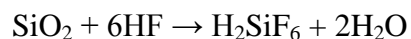


2) Direct dissolution of Si in divalent state



3) Si oxide formation followed by dissolution of oxide





Because of catalytic activity of the noble metal (silver in our case) , the oxidant is reduced at the surface of the noble metal. Now due to the reduction of the oxidant holes are generated. These generated holes then diffuse through the noble metal and are injected into the Si that is in contact with the noble metal. At the Si/metal interface, the injected hole oxidizes the Si and gets dissolved by HF. The reactant and the byproducts diffuse along the interface between the Si and the noble metal. The etching of Si by HF is much faster in the case where Si is in contact with the Si as the concentration of holes is maximum at the Si/metal interface than bare silicon without metal coverage.

Since the Fermi energy of Si substrate is less than the potential of Ag^+/Ag so when a silicon substrate was immersed into the HF/AgNO_3 solution, a galvanic cell was created. The injection of holes into valence band of Si from Ag^+ starts. Consequently, the Ag^+ was reduced to elemental Ag. The Ag nuclei size grew with increase in etching time while at the same time the local oxidation and dissolution of Si atoms is promoted by the holes injection into the valence band of Si with the help of Ag particles. The particles sank into the Si substrate with the dissolution of Si atoms underneath the Ag particles. At the interface between Si and the deposited Ag particle, the charge transfer happens and the Ag particles were formed by the reduction of Ag^+ at the bottom of the etched pores. Therefore, dendrite structures of Ag nuclei were formed. The diameter of the Si nanowire can be controlled by changing the concentration of the AgNO_3 and HF.

The metal taken as a catalyst has great influence upon the morphology of the etched structures [27]. It is reported that straight pores are formed if isolated Ag or Au particles are used as catalyst for etching the Si substrate but if Pt particles is used then defined straight pores or helical pores are formed. The type of noble

metal chosen may also affect the etching rate. Pt if used then the etching rate is more as compared to the etching rate if Au particles are used.

3.3 Raman and PL Spectroscopies

Raman experiments were carried out using Integrated Raman system that includes a confocal microscope, a large focal length (~800mm) having spectral resolution of $0.4 \text{ cm}^{-1}/\text{pixel}$ operating at the spectral range of 200–1050 nm and the source of excitation is 632.8 nm, air cooled He-Ne laser. The PL from MIE sample were recorded with 325 nm He-Cd laser excitation source using Dong Wooooptron 80K PL system at room temperature.

CHAPTER 4

Results and Discussion

This chapter deals with study of fabrication of SiNWs and pore characteristics of the samples prepared with the method of metal induced etching (MIE). Various types of analysis have been done for the better understanding of the pore formation and its dependence on different resistivity of Si.

4.1 SEM image analysis

As discussed earlier in section 2.2.4 PS/SiNWs of both type (n and p) can be fabricated by MIE and well aligned Si NWs can be formed. Important parameters like length, diameter, density and spacing can be controlled. As discussed earlier, two steps are involved in fabrication of PSi/SiNWs through MIE. Firstly, nanoparticles (NPs) of noble metal (in our case it is Ag) are deposited on Si substrate (wafer). Secondly, AgNPs deposited samples are dipped in the etching solution containing HF and H₂O₂. The area of Si substrate covered with Ag NPs is etched much faster due to catalysis effect, while the uncovered surface etches little slowly. Consequently, porous Si containing arrays of Si NWs are formed.

Fig. 4.1 shows an SEM image of Si Wafer. In MIE process, Ag is used as a catalyst to fasten up the etching process by dipping the Si substrate in the HF and H₂O₂ solution. An SEM image of that substrate has been taken and Fig. 4.2 clearly shows the deposition of AgNPs on the Si substrate when Si Wafer is kept in HF+AgNO₃ solution for 1 minute.

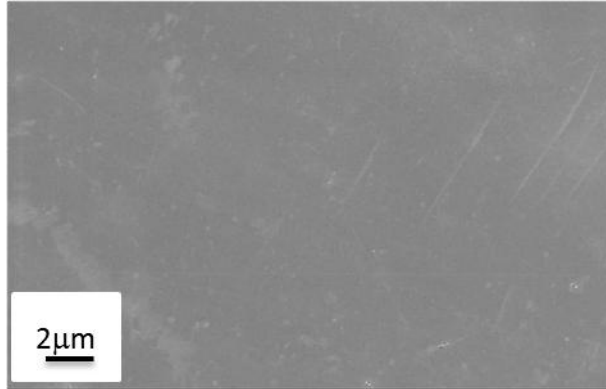


Fig. 4.1 SEM image of bare n type silicon substrate

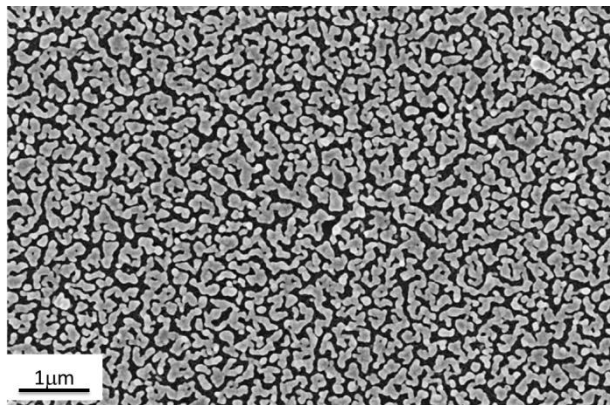


Fig. 4.2 Ag deposited on n-type Si substrate

The AgNPs deposited Si wafers have been used to prepare SiNWs using MIE technique. Nano walls like structures can be seen surrounding the AgNPs. SEM images after the removal of Ag particle of the sample were also taken for the same resistivity (Fig. 4.3). AgNPs seems to disappear completely from the Si substrate leaving behind only nanostructures of Si.

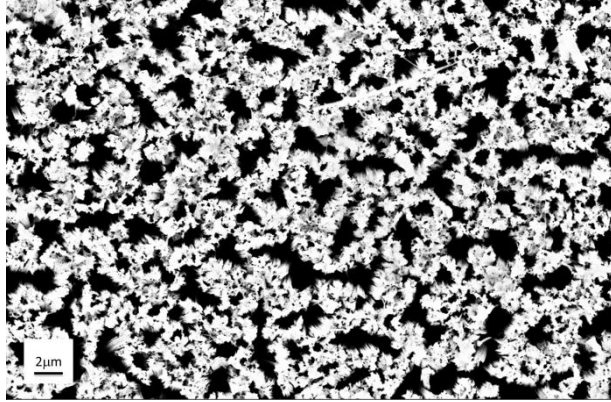


Fig. 4.3 SEM image of porosified Ag deposited Si-wafer.

Fig. 4.3 shows the porosified Ag deposited Si wafer. For this sample the etching time was 60 minute. To confirm wire like structure we have also done cross-sectional SEM. Fig 4.4 shows cross-sectional SEM image. The image clearly shows that wires of the order of few tens of nanometers have been formed.

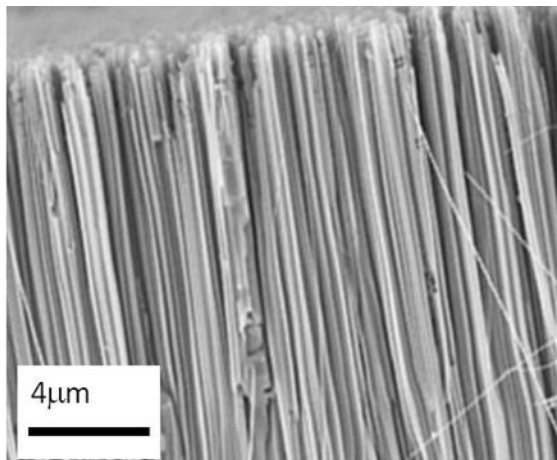


Fig. 4.4 Cross-sectional view of SiNWs prepared from n-type Si wafer.

The method of MIE is suitable not only to produce nanowires from n-type Si substrate but also in p-type. We have also prepared SiNWs in p-type Si substrate. Fig. 4.5 shows the top view of the prepared sample with etching time of 60

minute. Cross-sectional SEM image was also taken to confirm the formation of SiNWs in p-type wafer as shown in Fig 4.6.

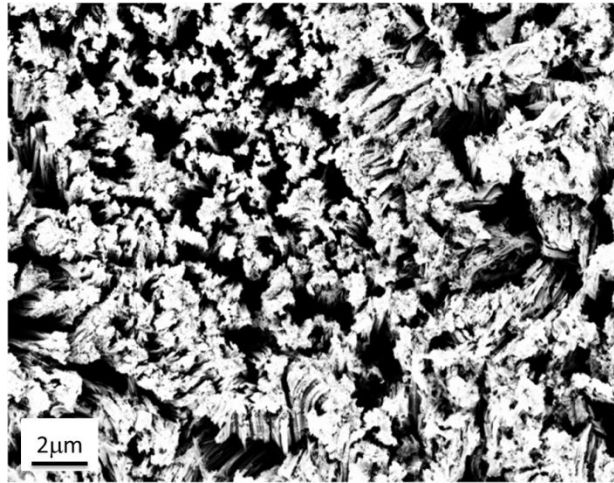


Fig 4.5 Top view of the etched p-type Si wafer for 60minute

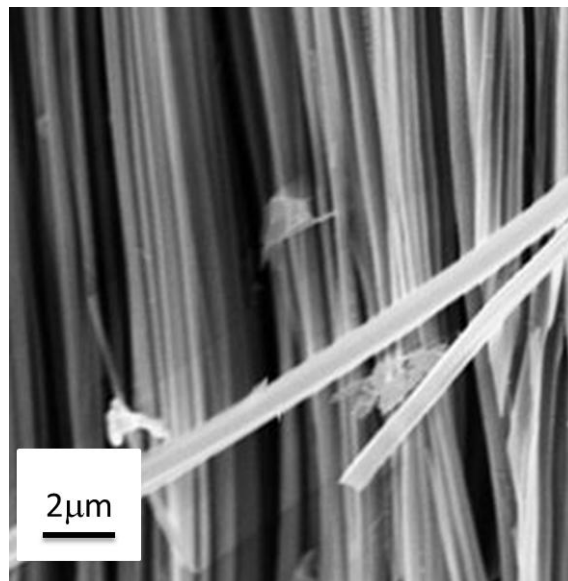


Fig. 4.6 Cross- Sectional SEM image of SiNWS formed on p-type Si substrate

4.2 Effect of etching time on porosification of Si

Surface morphologies of the sample have been studied using SEM in top/plane view as well as cross-sectional view to understand the progress of etching of Si

wafer and effect of etching time on porosity. Fig. 4.7 shows an SEM image corresponding to the porous Si samples fabricated from wafers with resistivity 1–20 Ωcm . Fig. 4.7 shows the top view, while Fig. 4.8 shows their corresponding cross-sectional images. These images indicate the formation of vertically aligned Si NWs arrays. The formation of such SiNWs is observed because H_2O_2 partially oxidises Ag NPs during etching to create a localized Ag^+ cloud. This Ag^+ cloud reacts quickly with Si and eject electrons near the Ag/Si interface. This is how the etching process initiates. After the starting of the process small pits are formed at the sites where Ag NPs are present and they get trapped in this pit. So, there is continued etching in vertical direction at the sites leading to the formation of the Si NWs array [28].

To study the effect of etching on porosification following samples have been prepared which are listed in table I.

Table I: Specification of samples for studying effect of etching on porosification of Si

Sample name	Etching time
E1	45 minutes
E2	60 minutes
E3	75 minutes

The effect of etching time on Si wafer in the same environment (other than etching time) can be understood from the SEM results which are shown in Fig.4.7- 4.8. The pore diameter and pore depth is expected to increase with increase in etching time [28]. But, as shown in Fig. 4.7-4.8, we have obtained quite an opposite result. In sample E1 (Fig. 4.7(a)), the diameter of Si NW arrays formed is found to be in range of few hundred nanometers after examining the planar view of SEM images. In the case of sample E3 the diameter of SiNW is bigger than sample E1. This indicates that after a particular etching time the diameter of SiNWs increase with the increasing etching time. Furthermore, from the observation of the X-section SEM images, the length of these Si NW arrays for the sample E1 (Fig. 4.8(a)) is found around 60 μm which is decreased upto a value 40 μm for E3 (Fig. 4.8(c)). Therefore, it can be asserted that after a particular etching time (60 minute in our case) breaking of the Si NWs started and results in blunt surface. On the contrary to our observation, it is reported [28] that length of the NWs increases from few nano-meters to several micrometers with increase in etching time from 0 to 120 minute and the increase in the length of Si NWs with the etching time is linear [28]. Hence, it can be concluded that in order to form well aligned SiNWs the optimum etching must be 45 minute for n-type Si wafer with 1–20 Ωcm resistivity. If duration of etching is elongated beyond this, NW arrays formed may get break.

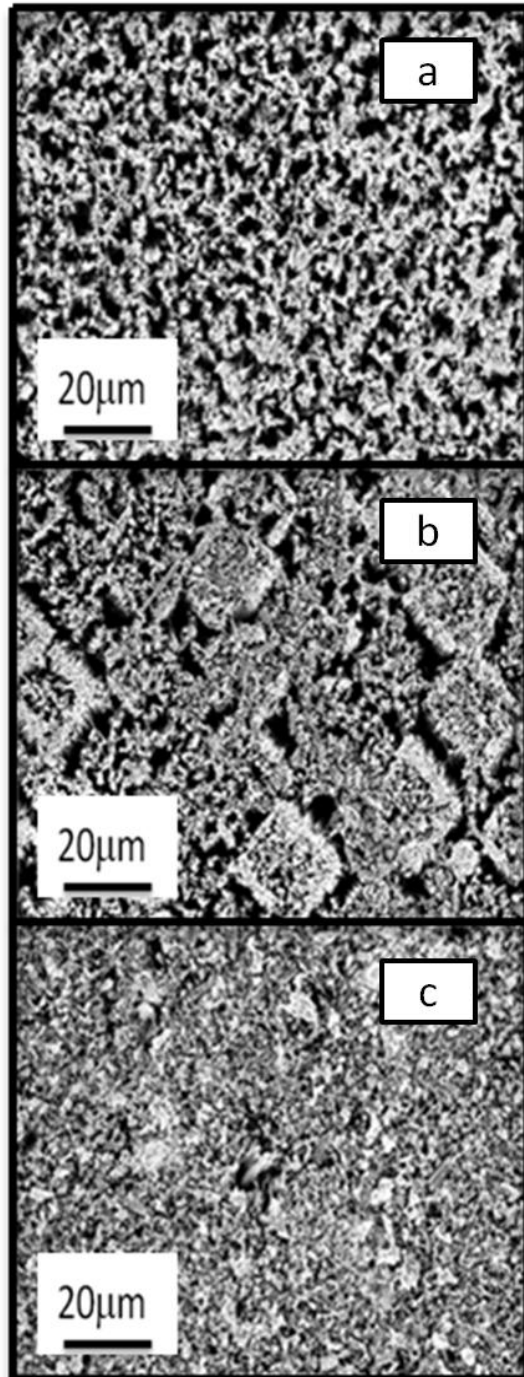


Fig. 4.7 Top view SEM image of sample (a) E1, (b) E2 and (c) E3

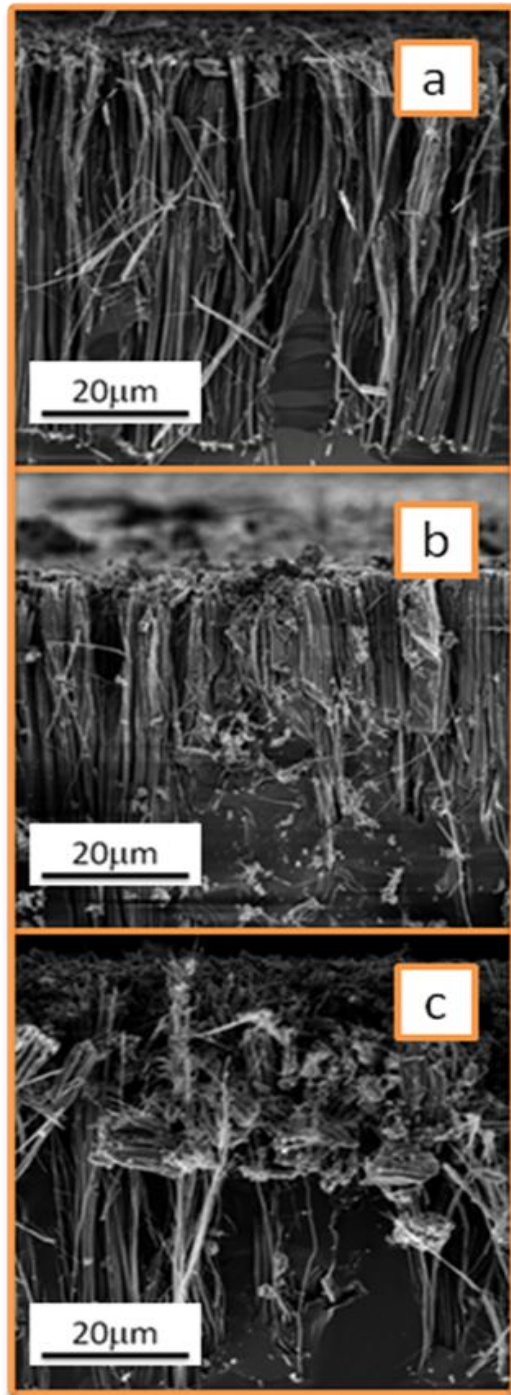


Fig. 4.8 Cross-sectional view of sample (a) E1 (b) E2 and (c) E3

4.3 Spectroscopic Investigation of SiNWs samples

4.3.1 Photoluminescence study of the samples

Photoluminescence (PL) measurements have been performed at room temperature using an excitation wavelength of 325 nm from He-Cd laser to see the luminescence properties of these formed Si nano-wire arrays. It has been observed that PL peak appears around 1.96 eV for the samples E1, E2 and E3 (Fig. 4.9). The variation in PL peak positions has been observed to be very little corresponding to a function of etching time. As we increase the etching time from 45 minute to 60 minute, a shift in PL peak position to higher energy is seen. Furthermore, if we increase etching time to 75 minute the PL energy gets reduced. It is in agreement with the SEM results which show that SiNWs with bigger diameter is formed in sample E3. Fig. 4.13 shows the PL peak positions for the samples E1, E2 and E3 appears to be at 1.95 (635.9 nm), 1.97 (629.4 nm) and 1.96 eV (632.6 nm) respectively. If we compare the diameter of nanowires in the sample E1 and E3, it is observed that diameter in case of sample E3 is bigger than that of sample E1 which is due to broken NW arrays.

As a consequence, for sample E3 a little red-shift in PL peak is observed compared to sample E1. As etching time is increasing from 45 to 60 minute PL intensity is increasing as more etching produce more luminescence sites but for the sample E3 intensity decrease because of broken SiNWs which reduces the number of luminescence sites.

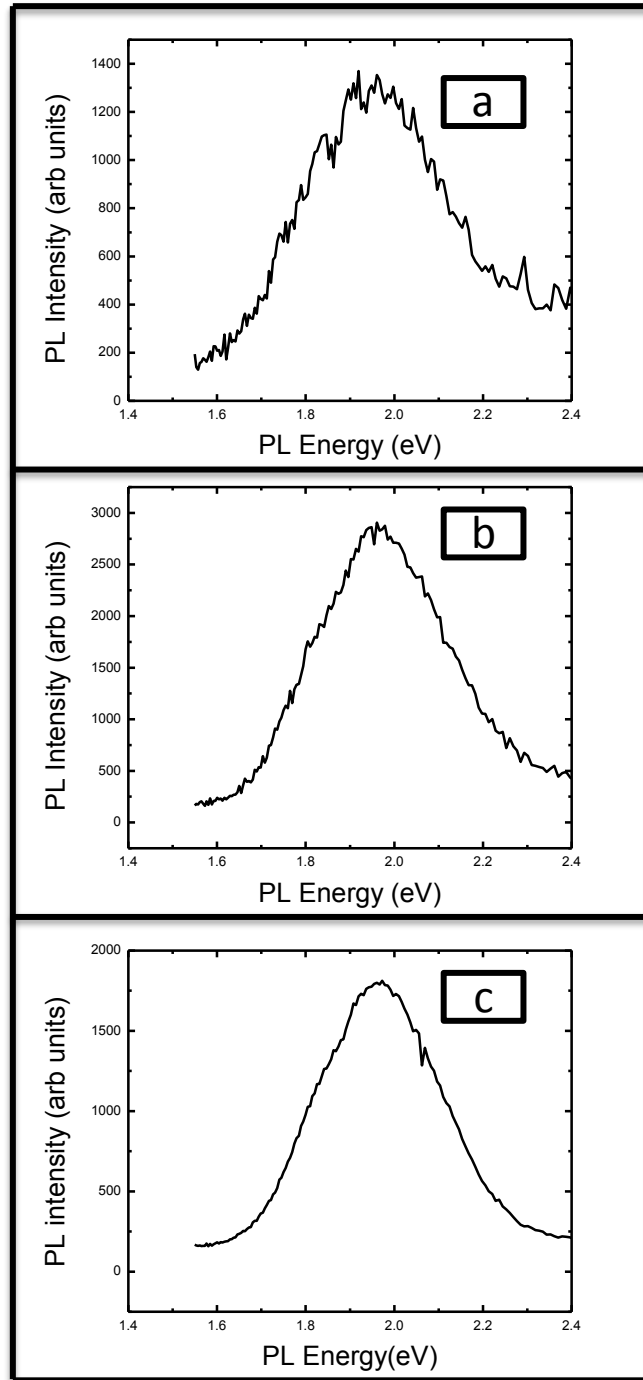


Fig. 4.9 PL spectra for (a) sample E1 (b) sample E2 (c) sample E3

4.3.2 Raman study of the Silicon

In order to estimate the average size of semiconductor nanostructures Raman spectroscopy has been done which is a popular tool for the characterization of nano materials [29]. In the case of crystalline bulk material only zone centre phonons ($q \approx 0$) contribute to first-order Raman scattering as a result symmetric Raman spectrum is achieved whereas $q \approx 0$ rule get relaxed in the case of quantum confined system. This implies that not only the zone centre optical phonons but the phonon away from the zone center ($q \geq 0$) can also contribute to the Raman scattering process. As a result of this, broaden asymmetric Raman spectra are achieved for nanostructures [29]. There are various models like phonon confinement model (PCM) [30], Bond-polarizability model (BPM) [31] etc. for fitting of Raman Spectra to find the important parameter to analyze the material properties. BPM is one of the simple methods to estimate the average size of nanostructures. Here we have used BPM due to its simplicity to estimate the average diameter of SiNWs of sample E1, E2, and E3.

Qualitative estimation of size of SiNWs by BPM can be obtained by the following relationship [31]:

$$\Delta\omega = \omega(L) - \omega_0 = -20.92(a/L)^{1.08}$$

In the above formula,

- 1) $\Delta\omega$ represents Red shift in Raman peak position.
- 2) $\omega(L)$ represents the frequency of Raman phonon of nanocrystal having size L.
- 3) ω_0 represents the frequency of the optical phonon corresponding to the zone centre.
- 4) ' a ' represents the lattice constant of c-Si.

Fig. 4.10 shows the Raman Spectra for sample E1, E2 and E3. Raman spectra shown in fig. 4.10 are red shifted, broad and asymmetric in nature as compared to its bulk counterpart (for C-Si 521 cm^{-1} shown by dotted lines). The Raman peak position for sample E1, E2 and E3 are 517.5 , 515 and 517 nm respectively. These peak positions have been used to estimate the average diameter of SiNW present in the sample E1, E2 and E3 and found to be 2.8 , 1.8 , and 2.5 nm respectively which are in the agreement with SEM and PL results.

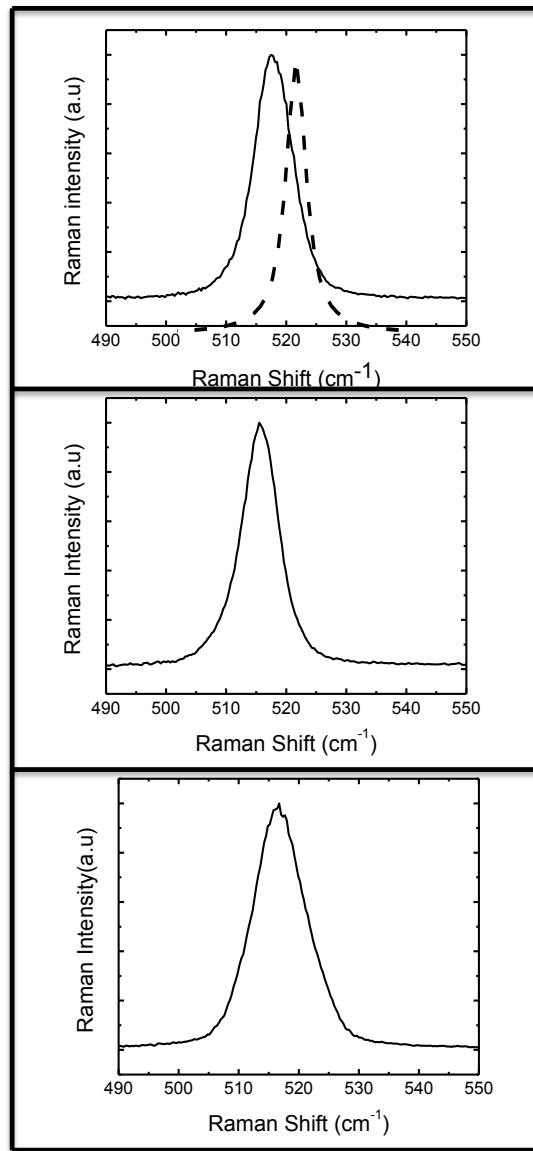


Fig. 4.10 Raman spectra for sample (a) E1 (b) E2 and (c) E3

4.4 Effect of AgNPs deposition time on porosification of Si

As already discussed in section 4.2 the Ag NPs plays a very significant role in the etching process because it initiates the porosification wherever Ag NPs get deposited. During the etching process these Ag NPs gets converted to Ag^+ ion . But these Ag^+ ions may get converted to Ag NPS again by accepting electrons from the wafer. Therefore, it is anticipated that resistivity of the Si wafer might have something to do with this. It has been reported that deposition of thicker Ag film results in the formation of columnar structures whereas fine pore structures has been observed with a layer of Ag film with nominal thickness [32]. To understand the effect of AgNPs size on porosification, following samples given on table II are prepared by varying AgNP deposition time. These AgNPs deposited Si Wafers are used for porosification to get a quantitative analysis of Ag sized dependent porosity.

TABLE II: Specification of the porous silicon samples prepared with n type ($0.01\Omega\text{cm}$) Si substrate.

Sample Name	Time of Ag deposition (sec)	Time of etching (min)
A	15	0
B	30	0
C	45	0
D	60	0
A60	15	60

Sample Name	Time of Ag deposition (sec)	Time of etching (min)
B60	30	60
C60	45	60
D60	60	60

The top view SEM image of the samples (Fig. 4.11) lucidly shows the Ag NPs being deposited on the substrate. As it can be seen from the SEM images (Fig. 4.11) that the density of Ag is increasing with deposition time. After dipping the samples in the etching solution and keeping the etching time constant for each sample SiNWs were prepared. SEM images of the etched samples with new series of sample (A60 to D60) are shown in Fig 4.12 and summarized in table IV. The porosity of these samples was calculated using ImageJ software.

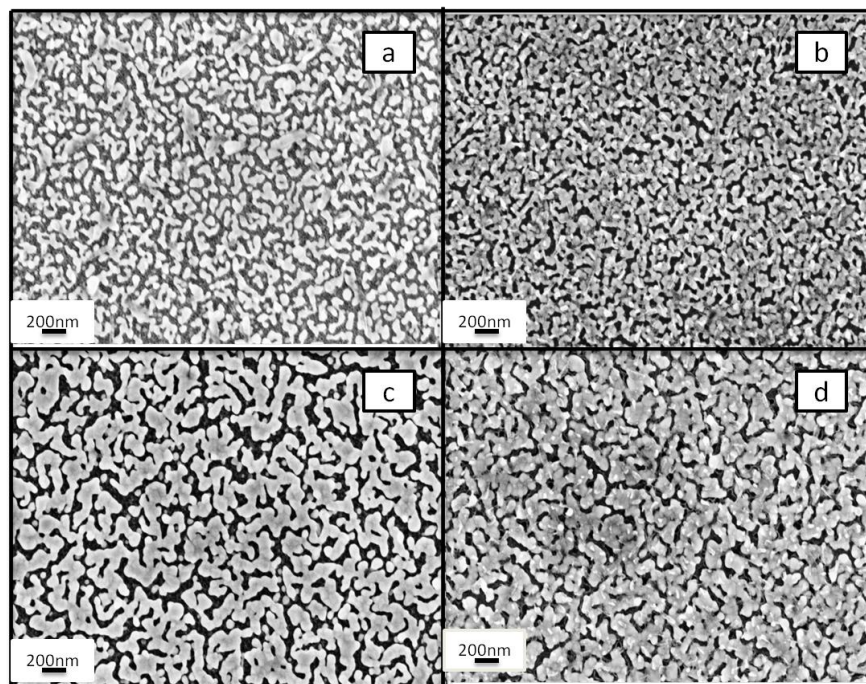


Fig. 4.11 SEM images of n (0.01 Ω cm) type Si substrate. Sample A to D showing variation in AgNPs.

Fig.4.12 shows the top view image of our sample. It can be observed from the SEM results that the pores have been formed in Si substrate. The sites where Ag NPs were deposited got etched significantly as discussed in section 4.1. It can be seen from the SEM results that pore formation is increasing from A60 to D60. Pore size in sample A60 is small and less dense. But in B60 the number of pores has increased leading to increase in porosity. Porosity has increased more in C60 as compared to B60 due to the increase in pore size as we can see big pores in the sample. Now in sample D60 more no of pores is formed which are comparatively larger in size and also denser than other samples (Fig 4.12 (d)).

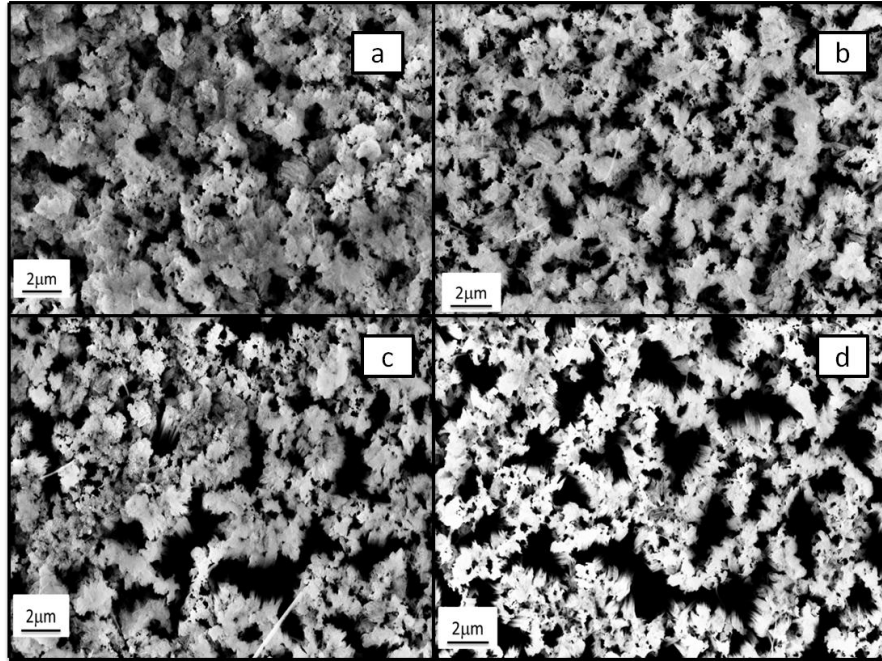


Fig. 4.12 SEM image of (a) A60, (b) B60, (c) C60 and (d) D60.

TABLE III: Specification of the porous silicon samples prepared with n type (0.01 Ω cm) Si substrate with only AgNPs deposition.

Sample name	Uncovered Area (%)	Covered Area (%)
A	44	56
B	36	64
C	31	69
D	27	73

TABLE IV: Specification of the porous silicon samples prepared n type (0.01 Ω cm) Si substrate after etching.

Sample name	porosity (%)
A60	22
B60	30
C60	35
D60	46

Process for obtaining the results is given in Appendix B.

Using Image-J software we have obtained percentage area which is not covered by AgNPs as summarized in Table III. It is evident from the table that the Ag deposition time is affecting the formation of pores in the Si substrate. The area covered by the Ag NPs in sample D is highest while in sample A it's the lowest. We observe here that in our samples deposition of Ag NPs in the Si substrate increases with time.

From table II, one can clearly see that the porosity is dependent on the Ag deposition time. As the etching time is constant, the porosity in n-type Si substrate with resistivity 0.01 Ω cm is increasing with Ag deposition time. In MIE technique Ag is used as catalyst to fasten the etching process and it is expected that greater the deposition of Ag greater should be the porosity which has been observed with our samples. Since, area covered by Ag was 56% in A60 sample which is the minimum as compared to B60, C60 and D60 sec the porosity of the same sample was the lowest among all other samples.

A plot of covered area vs. AgNPs deposition time has been plotted for the n type sample having resistivity 0.01 Ω cm with the help of Table III. The coverage area of the AgNPs is not varying linearly but is increasing slowly with time.

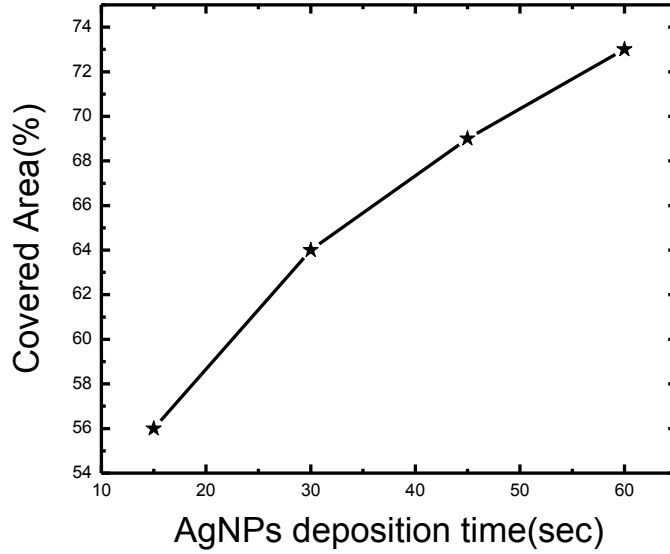


Fig. 4.13 Variation of covered area with Ag NPs deposition time.

Now the graph of porosity vs. AgNPs for the same samples has been plotted under the same conditions with the help of Table IV. Here also it is found that the porosity is increasing with AgNPs time but is not a linear increase.

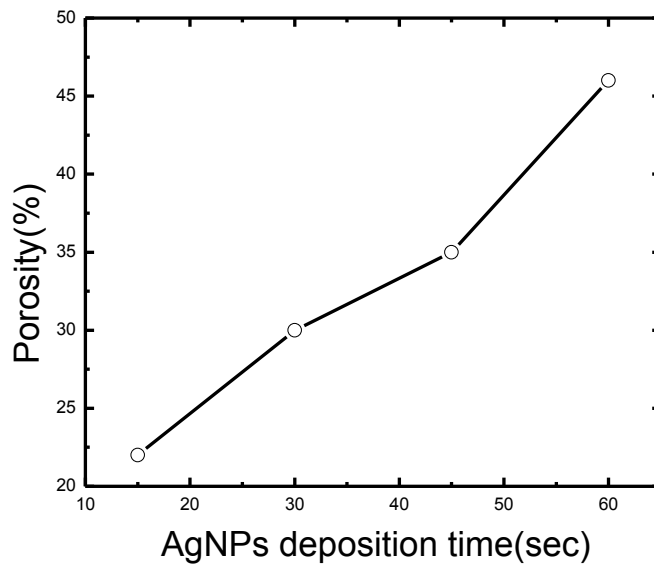


Fig. 4.14 Variation of porosity with Ag NPs deposition time

CHAPTER 5

Conclusion

A preliminary investigation on the formation of SiNWs has been presented. Optimization of initial surface pre-treatment is very significant such as cleaning and removing oxides, as well as post etching process. Well Aligned SiNWs are successfully fabricated by metal induced etching. Mechanism behind fabrication of SiNWs has been understood. A brief description about the method involved in the fabrication of SiNWs has been presented here. Surface morphology of different samples has been studied by SEM and cross-sectional. Effect of etching time on porosification of Si has been studied and shows after a particular etching time, SiNWs break that has been confirmed by cross-sectional SEM results. The effect of AgNPs deposition time on porosification of Si has been studied. Image J software is used to calculate the porosity of various samples. Porosity calculation provides the dependence of AgNPs deposition time on porosification of Si and shows that the porosity of different samples increases as AgNPs deposition time increases. Visible PL at room temperature shows the quantum confinement effect in the prepared samples which is the signature of nanostructures. Asymmetric and broad Raman spectra confirm the presence of nanostructures in the samples. Bond polarizability model is used to calculate the average size of nanostructures present in the samples. Particle size estimation shows the size of nanostructures decreases as etching time increases.

APPENDIX-A

Property	Value	Units
Atomic weight	28.09	
Atomic density	4.995×10^{14}	atoms/cm ²
Boiling point	2,878	°C
Breakdown field	3×10^5	V/cm
Bulk modulus	7.7×10^{11}	dynes/cm ²
Compliance<111>	5.32×10^{-13}	cm ² /dyne
Covalent radius	0.118	Nm
Critical density	0.1207	g/cm ³
Critical pressure	530	Atm
Critical temperature	4,886	°C
Critical volume	232.6	cm ³ /g.mol
Crystal plane spacing		
(100)	0.543	nm
(110)	0.383	nm
(111)	0.313	nm
Crystal structure	Diamond	
Density	2.33	g/cm ³

Property	Value	Units
Density of surface atoms		
(100)	6.78×10^{14}	atoms/cm ²
(110)	9.59×10^{14}	atoms/cm ²
(111)	7.83×10^{14}	atoms/cm ²
Dielectric constant	11.8	
Effective density of states		
Conduction band	3.22×10^{19}	n/cm ³
Valence band	1.83×10^{19}	n/cm ³
Elastic constant		
C ₁₁	1.29×10^{12}	
C ₁₂	0.483×10^{12}	
C ₁₄	0.671×10^{12}	
Electron affinity(111)	4.85	eV
Electron effective mass at 4 ⁰ K ^e		
Longitudinal (m _l /m ₀)	0.98	
Traverse (m _t /m ₀)	0.19	
Density of states(m [*] /m ₀)	1.08	

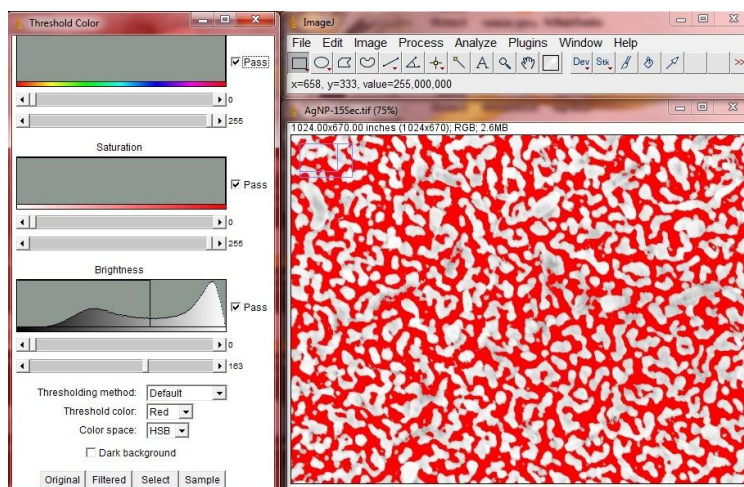
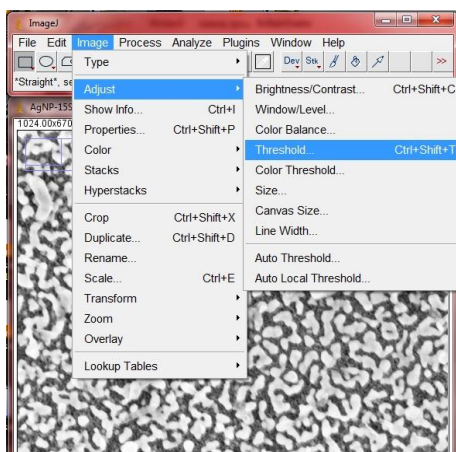
Property	Value	Units
Energy gap	1.12	eV
Hardness	7	Moh
Heat capacity	4.78	cal/g.mol ⁰ C
Heat of fusion	264	cal/g
Heat of sublimation	4,075.0	cal/g
Heat of vaporization	3,812.0	cal/g
Hole of effective mass at 4 ⁰ K [†]		
Heavy (m_1/m_0)	0.537	
Light (m_2/m_0)	0.153	
Density of states (m^*/m_0)	0.591	
Intrinsic carrier concentration		
n_i	1.38×10^{10}	n/cm ³
n_i^2	1.90×10^{20}	n/cm ³
Intrinsic Debye length		
L	28.7	μm
Ln_i	4.0×10^{-7}	n/cm ²
Intrinsic resistivity	2.3×10^5	Ω.cm
Lattice constant	0.543	Nm

Property	Value	Units
Liquid density	2.533	g/cm ³
Liquid heat capacity	6.755	cal/g.mol ⁰ C
Liquid thermal capacity	1.025x10 ⁻³	cal/sec.cm ⁰ C
Liquid viscosity	0.88	Centipoises
Melting point	1,412±2	⁰ C
Minority carrier lifetime	2.5x10 ⁻³	S
Nearest neighbor distance	0.235	Nm
Percent expansion on freezing	10%	
Poisson's ratio	0.27	
Refractive index	3.4	
Scattering limited velocity		
Electron	~1.0x10 ⁷	cm/s
Hole	~8.4x10 ⁶	cm/s
Shear modulus	7.55x10 ¹¹	dyne/cm ²
Surface tension	736	dynes/cm
Symbol	Si	

Property	Value	Units
Thermal conductivity	0.353	cal/sec.cm ⁰ C
Torsion modulus	3.97x10 ¹¹	dynes/cm ²
Vapor pressure	2.8x10 ⁻⁴	mm Hg

APPENDIX B

ImageJ software was used to calculate the results given in Table II. The SEM image for which porosity is to be estimated is selected and ‘Threshold’ command is clicked. This command is available via the menu command *Image>Adjust>Threshold*. Slider bars are available so that threshold can be set manually. The pixels within the threshold range are displayed in red. After satisfaction with the threshold settings, *Apply* the settings. The image gets converted to binary after the threshold settings are applied permanently. It then measures the porosity of the image using Measure command.



REFERENCES

- [1] Canham LT, Silicon quantum wire array fabrication by electrochemical and chemical dissolution of wafers. *Appl Phys Lett* , 1990, 5:1046-1048.
- [2] Cullis AG, Canham LT, Visible light emission due to quantum size effects in highly porous crystalline silicon. *Nature*, 1991, 353:335-338.
- [3] Cullis AG, Canham LT, Calcott PDJ, The structural and luminescence properties of porous silicon. *J Appl Phys*, 1997, 82:909-965.
- [4] Maier-Flaig F, Rinck J, Stephen M, et al. Multicolor Silicon Light-Emitting Diodes (SiLEDs). *Nano Lett.* , 2013, 13:475–480
- [5] Soref R, Silicon Photonics: A Review of Recent Literature. *Silicon*, 2010, 2:1-6.
- [6] Soref R ,Mid-infrared photonics in silicon and germanium. *Nat Photonics*, 2010, 4:495-497.
- [7] Chen R, Li D, Hu H, et al. , Tailoring Optical properties of Silicon Nanowires by Au Nanostructures Decorations: Enhanced Raman Scattering and Photodetection. *J Phys Chem C*, 2012, 116:4416-4422.
- [8] Letant S, Sailor MJ, Detection of HF Gas with a Porous Silicon Interferometer. *Adv Mater* , 2000, 12:355-359
- [9] Lin VS-Y, Motesharei K, Dancil K-PS, et al. A Porous Silicon Based Optical Interferometric Biosensor. *Science* , 1997, 278:840-843.
- [10] Canham LT , Bioactive silicon structure fabrication through nanoetching techniques. *Adv Matter* , 1995, 7:1033-1037.
- [11] Wang B, Cancilla JC, Torrecilla JS, Haick H , Artificial Sensing Intelligence with Silicon Nanowires for Ultrasensitive Detection in the Gas Phase. *Nano Lett* , 2014, 14:933–938.
- [12] Ge M, Rong J, Fang X, Zhou C , Porous Doped Silicon Nanowires for Lithium Ion Battery Anode with Long Cycle Life. *Nano Lett* , 2012, 12:2318–2323.
- [13] Zhao Y, Liu X, Li H, et al. Hierarchical micro/nano porous silicon Li-ion battery anodes. *Chem Commun* , 2012, 48:5079–5081.
- [14] Wei J, Buriak JM, Siuzdak G , Desorption–ionization mass spectrometry on porous silicon. *Nature* , 1999, 399:243–246.
- [15] Li Q, Koo S-M, Edelstein MD, et al. Silicon nanowire electromechanical switches for logic device application. *Nanotechnology*, 2007, 18:315202.
- [16] Wang B, Stelzner T, Dirawi R, et al. Field-Effect Transistors Based on Silicon Nanowire Arrays: Effect of the Good and the Bad Silicon Nanowires. *ACS Appl Mater Interfaces*, 2012, 4:4251–4258.
- [17] Anping Cao, Ernst J.R. Sudhölter, and Louis C.P.M. de Smet, *Sensors* (Basel). 2014 Jan; 14(1): 245–271

- [18] Kumar V, Saxena SK, Kaushik V, et al. Silicon nanowires prepared by metal induced etching (MIE): good field emitters. *RSC Adv* , 2014, 4:57799–57803.
- [19] Mingwang Shao, Dorothy Duo Duo Ma, and Shuit-Tong Lee, *Eur. J. Inorg. Chem.* 2010, 4264–4278
- [20] Jia Zhu , Zongfu Yu, George F. Burkhard, Ching-Mei Hsu, Stephen T. Connor, Yueqin Xu, Qi Wang, Michael McGehee, Shanhui Fan and Yi Cui, *Nano Lett.*, 2009, 9 (1), pp 279–282
- [21] Treuting, R. G.; Arnold, S. M. *Acta Met.* 1957, 5, 598.
- [22] Mehedhi Hasan, Md Fazlul Huq, Zahid Hasan Mahmood. *SpringerPlus*, 2013, 2:151
- [23] Zhipeng Huang, Nadine Geyer, Peter Werner, Johannes de Boor, and Ulrich Gösele. *Advanced Materials*, 2011, 23, 285–308
- [24] <http://science.howstuffworks.com/scanning-electron-microscope.htm>
- [25] Timothy H. Gfroerer “Photoluminescence in Analysis of Surfaces and Interfaces”, encyclopedia of Analytical Chemistry, John Wiley & Sons Ltd.
- [26] Linhan Lin, Siping Guo, Xianzhong Sun, Jiayou Feng and Yan Wang, *Nanoscale Research Letters*, 2010, 5:1822-1828
- [27] X.Li, P.W. Bohn. *Appl. Phys. Lett.* 2000, 77:2572
- [28] Srivastava SK, Kumar D, Singh PK, Kar M, Kumar V and Husain M., *Sol. Energy Mater. Sol. Cells*, 2010, 94:1506–11
- [29] Kumar R, Qualitative Evolution of Asymmetric Raman Line-Shape for NanoStructures, *Silicon*, 2014, 6:117-121
- [30] Richter H, Wang ZP, Ley L The one phonon Raman spectrum in microcrystalline silicon. *Solid State Commun* , 1981, 39:625–629.
- [31] Zi J, Büscher H, Falter C, Ludwig W, Zhang K, Xie X. Raman Shifts in Si Nanocrystals. *Appl. Phys. Lett.* 1996, 69: 200–202.
- [32] Cruz S, Honig-d’ Orville A and Muller J. *J. Electrochem*, 2005, Soc.152C418-24
- [33] Hiroshi Suzuki, Hiroshi Araki, Masahiro Tosa and Tetsuji Noda, *Materials Transactions*, 2007, 8:2202-2206
- [34] Werner P, Zakharov ND, Gerth G, Schubert L, Gösele U. *Int J Mater Res.* 2006, 97:1008–1015
- [35] Morales A.M. and Leiber C.M., *Science*, 1998, 279, 208-211.
- [36] Choy C.H, Cheah K.W. *Applied Physics A*, 1995, 61 :45-50
- [37] Zhang M-L, Peng K-Q, Fan X, Jie J-S, Zhang R-Q, Lee S-T and Wong N-B, *J. Phys. Chem.* 2008, C1124444–50

- [38] Yi, Gyu-Chul (Ed), *Semiconductor Nanostructures for Optoelectronic Devices*, Springer, 2012
- [39] Lin L, Guo S, Sun X, Feng J and Wang Y, *Nanoscale Res. Lett.*, 2010, 5: 1822
- [40] Qu Y, Zhou Hand DuanX, *Nanoscale*, 2011, 3: 4060–8
- [41] Kuan-I Chen, Bor-Ran Li, Yit-Tsong Chen, *Nano Today*, 2011, 6:131-154
- [42] Yoni Engel, Roey Elnathan, Alexander Pevzner, Guy Davidi, Eli Flaxer and Fernando Patolsky, 2010, 38:6830-6835
- [43] Eman Sad Ashour, Mohamad Yusof Bin Sulaiman, Mohd Hafidz Ruslan and Kamaruzzaman Sopian, *Nanoscale Research Letters*, 2013, 8:466